

# COMPOSED VISION-LANGUAGE RETRIEVAL FOR SKIN CANCER CASE SEARCH VIA JOINT ALIGNMENT OF GLOBAL AND LOCAL REPRESENTATIONS

Yuheng Wang<sup>1</sup> Yuji Lin<sup>2</sup> Dongrun Zhu<sup>2</sup> Jiayue Cai<sup>2,\*</sup> Sunil Kalia<sup>1</sup>  
Harvey Lui<sup>1</sup> Chunqi Chang<sup>2</sup> Z. Jane Wang<sup>1</sup> Tim K. Lee<sup>1</sup>

<sup>1</sup> The University of British Columbia, Vancouver, BC, Canada V6T 1Z4

<sup>2</sup> Shenzhen University, Shenzhen, Guangdong, China, 518055

## ABSTRACT

Medical image retrieval aims to identify clinically relevant lesion cases to support diagnostic decision making, education, and quality control. In practice, retrieval queries often combine a reference lesion image with textual descriptors such as dermoscopic features. We study composed vision–language retrieval for skin cancer, where each query consists of an image–text pair and the database contains biopsy-confirmed, multi-class disease cases. We propose a transformer-based framework that learns hierarchical composed query representations and performs joint global–local alignment between queries and candidate images. Local alignment aggregates discriminative regions via multiple spatial attention masks, while global alignment provides holistic semantic supervision. The final similarity is computed through a convex, domain-informed weighting that emphasizes clinically salient local evidence while preserving global consistency. Experiments on the public Derm7pt dataset demonstrate consistent improvements over state-of-the-art methods. The proposed framework enables efficient access to relevant medical records and supports practical clinical deployment.

**Index Terms**— Skin cancer, composed image retrieval, vision-language retrieval, dermatology, global and local alignment.

## 1. INTRODUCTION

Early screening and diagnosis of skin cancer enable timely treatment planning, reducing patient morbidity and improving cure rates [1]. Achieving these benefits, however, depends on accurate interpretation of often subtle lesion appearances. With rapid advances in artificial intelligence, deep learning-based classification systems have reached dermatologist-level performance in multiple settings [2, 3, 4]. However, a central challenge remains translating these models into routine clinical workflows. Compared with end-to-end classification, case-based retrieval offers a more clinically intuitive form

\* indicates the corresponding author.

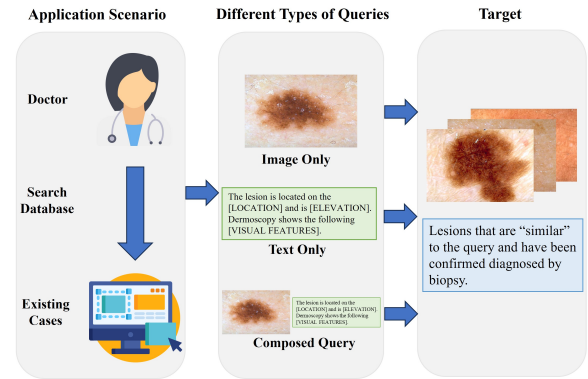


**Fig. 1.** Types of clinical skin cancer case search and query. Conventional retrieval uses image-only queries or text-only clinical descriptors separately, whereas our composed retrieval pairs a reference lesion image with its associated text to form a vision-language query. All settings aim to retrieve visually similar, biopsy-confirmed cases from an image-only database to support clinical decision making.

of decision support by comparing similar historical cases, thereby facilitating comparative assessment, interpretability, and clinician training [5]. In practice, clinicians generally formulate retrieval queries by pairing a reference lesion image with concise textual descriptions (e.g., dermoscopic patterns or checklist-based criteria) [6]. Thus, constructing effective vision–language hybrid queries that fully exploit multimodal information is critical to enabling practical, trustworthy skin cancer decision support.

Over the past five years, transformer architectures, which are well suited to modeling long-range dependencies in sequential data, have driven major advances in large-scale semantic prediction models [7, 8, 9, 10]. Building on these developments, vision transformers have further reshaped performance benchmarks in computer vision by enabling effective global context modeling in images [11, 12]. These advances provide a strong technical foundation for multimodal composed image retrieval, where visual and textual cues can be integrated into a unified representation for reliable case match-

ing [13, 14].

Based on the above motivation and background, we study transformer-based composed vision-language retrieval for skin cancer case search, where each query pairs a reference lesion image with accompanying clinical text to retrieve relevant cases from an image database. The key challenge is to design a clinically meaningful similarity function that captures global semantics (e.g., overall lesion morphology and color distribution) while emphasizing localized discriminative cues (e.g., streaks, irregular pigmentation, and regression-like structures). We address this by learning multi-level composed query representations via image and text fusion and matching them to target images through joint global-local similarity alignment, enabling robust case ranking for clinical assessment. Our main contributions are as follows:

- We formulate skin cancer case search as a composed vision-language retrieval problem, where each query pairs a reference lesion image with its associated clinical text to retrieve relevant target images from the existing database. To the best of our knowledge, this is the first study to investigate composed image retrieval for skin cancer case search.
- We introduce and adapt a hierarchical representation learning framework with joint global-local alignment for skin cancer retrieval, where learnable region masks capture discriminative local patterns and a weighted global-local similarity emphasizes clinically relevant details.
- We conduct extensive experiments on a publicly available multimodal skin lesion dataset and demonstrate state-of-the-art retrieval performance.

## 2. METHOD

### 2.1. Problem formulation

Let the image database be  $\mathcal{D} = \{(I_n, y_n)\}_{n=1}^N$ , where  $I_n$  denotes a lesion image and  $y_n$  is its diagnostic label. A retrieval query is defined as  $q = (I_q, T_\tau, y_q)$ , consisting of a *query* image  $I_q$  and a textual description  $T_\tau$  (e.g., checklist-based criteria) associated with the query label  $y_q$ . We define label-level positives  $\mathcal{P}$  as

$$\mathcal{P}(q) = \{n \mid y_n = y_q\} \quad (1)$$

Given  $q$ , our goal is to learn a similarity function  $S(q, I_n)$  that ranks all database images  $I_n$  and returns the top- $K$  most relevant cases with the same diagnosis label. This formulation reflects the clinical workflow where the image provides morphological context while the text specifies discriminative diagnostic cues.

### 2.2. Overview

Fig. 2 illustrates the overall workflow of our framework. Given a composed query  $q = (I_q, T_\tau, y_q)$  and a candidate target image  $I_t$ , our model computes a multi-level similarity by integrating (i) hierarchical visual representations, (ii) cross-modal composition between  $I_q$  and  $T_\tau$ , and (iii) joint global/local alignment between the composed query and  $I_t$ . Concretely, we first extract multi-level feature maps from both reference and target images using a hierarchical vision backbone. We then fuse the reference-image features with text token embeddings via a cross-modal Transformer to obtain a *composed* query representation at each feature level. Finally, we measure query-target similarity through complementary global and local alignment terms: global alignment captures overall semantics and provides stable supervision, whereas local alignment emphasizes region-level discriminative patterns that are critical for clinical diagnosis.

### 2.3. Hierarchical visual encoding

As illustrated in Fig. 2(a), we use a hierarchical vision backbone built on the Swin Transformer [11] to extract multi-level visual features, following the practice in prior composed retrieval frameworks [12]. The extracted multi-level visual features  $f_{\text{vis}}$  from an image  $I$ :

$$\{X^L(I), X^M(I), X^H(I)\} = f_{\text{vis}}(I) \quad (2)$$

where  $X^L \in \mathbb{R}^{h_L \times w_L \times d_L}$ ,  $X^M \in \mathbb{R}^{h_M \times w_M \times d_M}$ , and  $X^H \in \mathbb{R}^{h_H \times w_H \times d_H}$  denote low-, middle-, and high-level feature maps, respectively. These hierarchical representations preserve both fine-grained appearance details and higher-level semantic context, which are jointly necessary for robust lesion matching. For the query image  $I_q$  and a target database image  $I_t$ , we compute

$$X_q^i = X^i(I_q), \quad X_t^i = X^i(I_t), \quad i \in \{L, M, H\} \quad (3)$$

### 2.4. Text encoding and cross-modal composition

Given the textual description  $T_\tau$ , we employ BERT as the language encoder to obtain token embeddings, following the text encoding setup in [15]:

$$Z_\tau = f_{\text{text}}(T_\tau) \in \mathbb{R}^{n \times d_T} \quad (4)$$

where  $n$  is the number of tokens and  $d_T$  is the token embedding dimension. To construct a composed query that reflects both the reference appearance and the specified textual attributes, we employ a cross-modal Transformer that injects textual information into the reference visual features. For each feature level  $i \in \{L, M, H\}$ , we compute

$$X_{q\tau}^i = \text{CrossTransformer}(X_q^i, Z_\tau) \quad (5)$$

where  $X_{q\tau}^i \in \mathbb{R}^{h_i \times w_i \times d_i}$  denotes the composed query feature map at level  $i$ , expressed in the same visual feature space as  $X_t^i$  to enable direct query-target alignment.

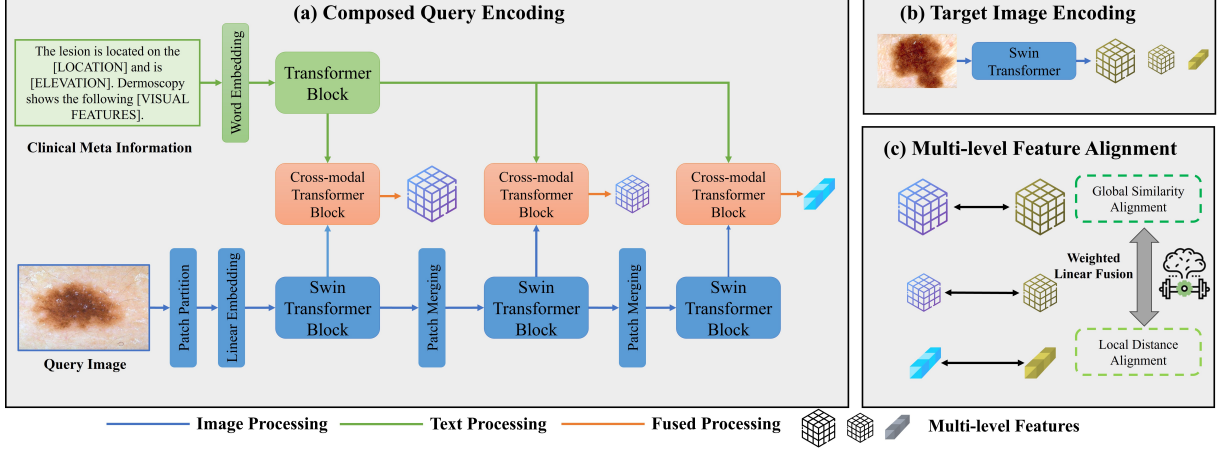


**Fig. 2.** Overall workflow of composed vision-language retrieval for skin cancer. The query image and text are fused via cross-modal Transformers on top of a hierarchical vision backbone to form multi-level composed query representations (a), while each database image is encoded by the same backbone (b). Multi-level global and local alignment jointly compute query-target similarity for retrieval ranking (c).

## 2.5. Joint alignment of multi-level representations

We quantify the similarity between the composed query  $\{X_{q\tau}^i\}$  and the target image features  $\{X_t^i\}$  via two complementary terms. Global alignment compares pooled representations to capture overall lesion-level semantics (e.g., morphology and color distribution). Local alignment, in contrast, focuses on discriminative subregions (e.g., streaks, irregular pigmentation, regression-like patterns) by learning multiple region masks and aggregating region descriptors. Combining these two views yields a similarity function that is both semantically coherent and locally sensitive.

Firstly, we model local discriminative patterns by learning  $k$  region masks and aggregating region descriptors. For each feature level  $i \in \{L, M, H\}$  and region index  $j \in \{1, \dots, k\}$ , a region descriptor is computed as

$$E_{ij} = \rho(X^i \odot \alpha_j(X^i)) \quad (6)$$

where  $\alpha_j(\cdot) \in \mathbb{R}^{h_i \times w_i \times 1}$  produces a spatial attention mask,  $\odot$  denotes Hadamard product, and  $\rho(\cdot)$  is a pooling operator yielding a  $d_i$ -dimensional vector. Applying Eq. (6) to  $X_{q\tau}^i$  and  $X_t^i$  yields region sets  $E_{q\tau}^i \in \mathbb{R}^{k \times d_i}$  and  $E_t^i \in \mathbb{R}^{k \times d_i}$ . We then compute the local similarity by aggregating the  $k$  region descriptors and measuring cosine similarity:

$$S_{\text{local}} = \sum_{i \in \{L, M, H\}} s(\rho(E_{q\tau}^i), \rho(E_t^i)) \quad (7)$$

where  $s(\cdot, \cdot)$  denotes cosine similarity and  $\rho(\cdot)$  aggregates region descriptors (e.g., average over  $k$ ). This formulation encourages the model to align diagnostically informative patterns without requiring explicit lesion-level annotations.

For the global alignment, to capture overall semantics and provide stable supervision complementary to local matching,

we compute a global similarity by pooling each feature map and applying cosine similarity:

$$S_{\text{global}} = \sum_{i \in \{L, M, H\}} s(\rho(X_{q\tau}^i), \rho(X_t^i)) \quad (8)$$

Global alignment emphasizes holistic consistency between the composed query and the target image, and empirically helps stabilize the learning of local attention masks by preventing degenerate region selections.

We then combine the local and global similarities via a weighted aggregation to obtain the final query-target similarity score:

$$S = \beta S_{\text{local}} + (1 - \beta) S_{\text{global}} \quad (9)$$

where  $\beta \in [0, 1]$  governs the trade-off between local and global signals, and a larger  $S$  indicates a stronger query-target match. In skin cancer case search, diagnostically salient cues are frequently confined to specific lesion subregions (e.g., streaks, irregular pigmentation, and regression-like patterns); accordingly, we choose a  $\beta$  that prioritizes  $S_{\text{local}}$  while using  $S_{\text{global}}$  as a holistic semantic constraint.

This design departs from prior composed/image retrieval methods that predominantly rely on global embedding similarity [5, 6] or perform global-local aggregation without accounting for domain-dependent cue reliability [12]. By embedding this clinical reliability prior into a simple convex fusion, our similarity better aligns with medical decision patterns without sacrificing global consistency.

Meta Report Template
The lesion is located on the [LOCATION] and is [ELEVATION].
Dermoscopy shows [DOTS_GLOBULES_PHRASE]; [BLUE_WHITE_PHRASE];
[PIGMENT_NETWORK_PHRASE]; [STREAKS_PHRASE]; [PIGMENTATION_PHRASE];
[REGRESSION_PHRASE]; and [VASCULAR_PHRASE].
Seven-point checklist score: [SEVEN_POINT_SCORE] (level of concern: [LEVEL_OF_CONCERN]).
Planned management: [MANAGEMENT].

Fig. 3. Meta report template used to construct textual queries.

### 3. EXPERIMENTS

#### 3.1. Benchmark dataset

We selected Derm7pt, a widely used benchmark for skin cancer research, because it provides dermoscopic images alongside patient metadata and structured clinical attributes aligned with the 7-point checklist [16]. Following prior retrieval-oriented studies, we adopted the standard evaluation protocol for retrieval on this dataset. To ensure sufficient class representation and reliable performance estimation, we restricted analysis to diagnostic categories with at least 50 samples [5]. Under this criterion, Derm7pt yields 888 eligible images from the original 1,011, spanning three categories: melanoma (mel), nevus, and benign keratosis-like lesions (bkl). For the original settings of the dataset, each image has a maximum resolution of  $768 \times 512$  pixels. To minimize format-dependent variability, we first removed black boundary artifacts and then resized all images to  $512 \times 512$  pixels, enabling efficient use of image content while preventing unnecessary information loss. Since our method uses only dermoscopy images and meta information, we ensured fair comparisons with state-of-the-art approaches by adopting the same input setting. Specifically, for methods requiring image and metadata inputs (e.g., SNF-DCA), we consistently used dermoscopy images together with the associated meta information, and excluded clinical photographs from the dataset for all methods. In the training phase, we adopted five-fold cross-validation to obtain reliable performance estimates under the limited dataset size. We set the number of epochs to 100 and employed the Adam optimizer with a learning rate of  $10^{-4}$  and a weight decay of  $10^{-5}$ . Early stopping was applied with a patience of 30 epochs. The weighting coefficient  $\beta$  in Eq. (9) was set as 0.6 based on preliminary experiments.

#### 3.2. Evaluation metrics

We assess retrieval performance using mean Average Precision (mAP) and Accuracy@ $K$  following standard practice in prior work.

Given a query  $q$  and its ranked retrieval list  $\{r_1, r_2, \dots, r_N\}$ , we define an indicator  $rel(i) = 1$  if item  $r_i$  is relevant to  $q$ ,

Table 1. Accuracy@ $K$  overall performance across 5-fold cross-validation (Mean  $\pm$  Std, in %).

Method	Acc@1	Acc@2	Acc@4
ResNet50-CosSim [5]	77.6 $\pm$ 3.5	80.9 $\pm$ 2.6	83.2 $\pm$ 1.9
SNF-DCA [6]	77.8 $\pm$ 2.3	82.8 $\pm$ 1.4	83.3 $\pm$ 2.5
MaskRCNN-Fusion [17]	62.5 $\pm$ 1.2	77.3 $\pm$ 3.1	<b>87.3 <math>\pm</math> 2.5</b>
DAHNET [18]	74.4 $\pm$ 2.1	74.9 $\pm$ 1.8	75.6 $\pm$ 2.7
Proposed	<b>79.3 <math>\pm</math> 2.9</b>	<b>82.4 <math>\pm</math> 3.6</b>	<b>87.3 <math>\pm</math> 3.2</b>

Table 2. Mean Average Precision (mAP) for each fold and overall performance across 5-fold cross-validation (in %).

Method	Fold 1	Fold 2	Fold 3	Fold 4	Fold 5	Mean $\pm$ Std
ResNet50-CosSim [5]	78.5	81.7	<b>84.0</b>	77.2	80.6	80.4 $\pm$ 2.7
SNF-DCA [6]	79.4	81.6	80.4	80.1	78.4	80.0 $\pm$ 1.2
MaskRCNN-Fusion [17]	61.3	57.8	60.4	61.5	61.2	60.5 $\pm$ 1.5
DAHNET [18]	79.1	80.5	81.6	<b>80.2</b>	<b>81.5</b>	80.6 $\pm$ 1.0
Proposed	<b>83.8</b>	<b>84.5</b>	82.4	78.6	79.3	<b>81.7 <math>\pm</math> 2.7</b>

and 0 otherwise. The precision at rank  $i$  is:

$$P(i) = \frac{\sum_{j=1}^i rel(j)}{i}. \quad (10)$$

The Average Precision (AP) for query  $q$  aggregates the precision values at all positions where relevant items appear:

$$AP(q) = \frac{1}{R_q} \sum_{i=1}^N P(i) rel(i), \quad (11)$$

where  $R_q$  is the number of relevant items for query  $q$ . The final mAP score is the mean AP across all queries:

$$mAP = \frac{1}{Q} \sum_{q=1}^Q AP(q), \quad (12)$$

where  $Q$  denotes the total number of queries. mAP thus evaluates the overall ranking quality by rewarding relevant items that appear earlier in the list.

Accuracy@ $K$  examines whether at least one relevant item appears within the top- $K$  retrieved results. For each query  $q$ ,

$$Acc@K(q) = \begin{cases} 1, & \exists i \leq K \text{ such that } rel(i) = 1, \\ 0, & \text{otherwise,} \end{cases} \quad (13)$$

and

$$Accuracy@K = \frac{1}{Q} \sum_{q=1}^Q Acc@K(q). \quad (14)$$

## 4. RESULTS AND DISCUSSION

### 4.1. Quantitative results

We compare against ResNet50-CosSim [5] as the dataset benchmark baseline, SNF-DCA [6] as the first multimodal

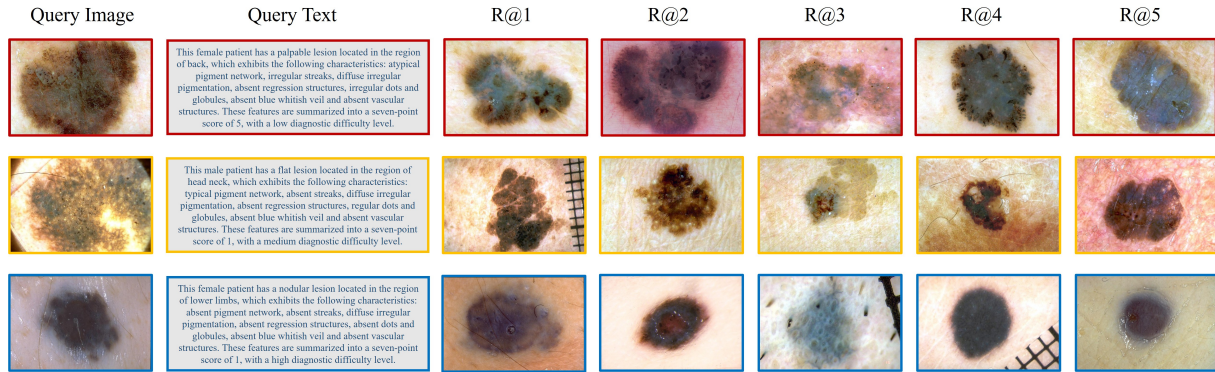


**Fig. 4.** Qualitative composed retrieval examples on Derm7pt. Each row shows one query (left: query image; middle: associated clinical text) and the top-5 retrieved images (right, R@1–R@5). Rows 1–3 correspond to mel (red borders), bkl (yellow borders), and nevus (blue borders), respectively.

retrieval method on this dataset, MaskRCNN-Fusion [17] as a recent skin-specific retrieval approach, and DAHNET [18] as the recent state of the art retrieval study. As shown in Table 1, our method achieves the best average Accuracy@{1, 2, 4} (83.0%), improving upon SNF-DCA (81.3%) and ResNet50-CosSim (80.6%). Relative to conventional global embedding retrieval (ResNet50-CosSim, 80.6%), the improvement is 2.4%, indicating that incorporating textual attributes into the query and jointly aligning global and local representations yields a more discriminative similarity function than purely appearance-driven matching. More importantly, the advantage is most evident at the strict top-1 setting: our Accuracy@1 reaches 79.3%, compared with 77.8% for SNF-DCA and 77.6% for ResNet50-CosSim. This improvement suggests that emphasizing localized diagnostic cues during matching can better resolve fine-grained ambiguity among visually similar lesions, which is critical for clinical decision support where the first returned case often has the highest practical impact. At a larger  $K$ , the strong Acc@4 (87.3%) yet weak Acc@1 (62.5%) of MaskRCNN-Fusion suggests that segmentation-driven fusion may retrieve relevant cases within the top few results yet struggles to produce consistently correct top-ranked matches, whereas our approach improves early precision by aligning clinically meaningful local patterns with global semantic consistency.

Table 2 further supports these observations from a ranking-quality perspective. Our method achieves the highest mean mAP (81.7%), surpassing DAHNET (80.6%), ResNet50-CosSim (80.4%), and SNF-DCA (80.0%). The mAP gains indicate that improvements are not limited to a single cut-off  $K$ , but instead reflect more coherent ordering of relevant cases throughout the ranked list. Collectively, these results highlight the benefit of composed querying in clinical retrieval: fusing query images with structured clinical descriptors and prioritizing local discriminative evidence yields more reliable top-ranked case retrieval while maintaining

strong overall ranking quality, thereby better matching the needs of real-world skin cancer case search.

#### 4.2. Qualitative analysis

Fig. 4 presents representative composed retrieval results on Derm7pt. For each query, the model integrates a reference lesion image with its associated clinical text and returns the top-5 most similar cases from the image database. Overall, the retrieved cases are visually and clinically consistent with the queries: for the melanoma example (Row 1, red), top-ranked results preserve key malignant cues such as heterogeneous pigmentation and irregular structures; for the bkl example (Row 2, yellow), retrieved lesions exhibit characteristic keratotic appearance and coarse texture patterns; and for the nevus example (Row 3, blue), the returned cases show more regular and homogeneous pigmentation with smoother boundaries. Notably, the top-ranked predictions in each row remain coherent across R@1–R@5, suggesting that the proposed local-emphasized similarity effectively captures discriminative substructures while global similarity maintains overall morphological consistency. These observations align with the quantitative gains in early-rank metrics, supporting that the framework retrieves clinically relevant analogues that are suitable for comparative assessment in case-based decision support.

## 5. CONCLUSION

We investigate composed image retrieval for skin cancer case search, where each query pairs an image with clinical text to retrieve relevant cases from an image database of biopsy-confirmed diagnoses. Our approach learns hierarchical composed representations and ranks targets using a weighted global-local similarity that balances holistic semantics with discriminative local cues. By returning clinically comparable, biopsy-confirmed cases, the framework provides intuitive decision support and enables efficient access to evidence.

## 6. REFERENCES

- [1] M Emre Celebi, Noel Codella, and Allan Halpern, “Dermoscopy image analysis: overview and future directions,” *IEEE journal of biomedical and health informatics*, vol. 23, no. 2, pp. 474–478, 2019.
- [2] Andre Esteva, Brett Kuprel, Roberto A Novoa, Justin Ko, Susan M Swetter, Helen M Blau, and Sebastian Thrun, “Dermatologist-level classification of skin cancer with deep neural networks,” *nature*, vol. 542, no. 7639, pp. 115–118, 2017.
- [3] Catarina Barata, Veronica Rotemberg, Noel CF Codella, Philipp Tschandl, Christoph Rinner, Bengu Nisa Akay, Zoe Apalla, Giuseppe Argenziano, Allan Halpern, Aimilios Lallas, et al., “A reinforcement learning model for ai-based decision support in skin cancer,” *Nature Medicine*, vol. 29, no. 8, pp. 1941–1946, 2023.
- [4] Siyuan Yan, Zhen Yu, Clare Primiero, Cristina Vico-Alonso, Zhonghua Wang, Litao Yang, Philipp Tschandl, Ming Hu, Lie Ju, Gin Tan, et al., “A multimodal vision foundation model for clinical dermatology,” *Nature Medicine*, pp. 1–12, 2025.
- [5] Philipp Tschandl, Giuseppe Argenziano, Majid Razmara, and Jordan Yap, “Diagnostic accuracy of content-based dermatoscopic image retrieval with deep classification features,” *British Journal of Dermatology*, vol. 181, no. 1, pp. 155–165, 2019.
- [6] Yuheng Wang, Nandinee Fariah Haq, Jiayue Cai, Sunil Kalia, Harvey Lui, Z Jane Wang, and Tim K Lee, “Multi-channel content based image retrieval method for skin diseases using similarity network fusion and deep community analysis,” *Biomedical Signal Processing and Control*, vol. 78, pp. 103893, 2022.
- [7] Ashish Vaswani, Noam Shazeer, Niki Parmar, Jakob Uszkoreit, Llion Jones, Aidan N Gomez, Lukasz Kaiser, and Illia Polosukhin, “Attention is all you need,” *Advances in neural information processing systems*, vol. 30, 2017.
- [8] Mikhail V Korotееv, “Bert: a review of applications in natural language processing and understanding,” *arXiv preprint arXiv:2103.11943*, 2021.
- [9] Laila Rasmy, Yang Xiang, Ziqian Xie, Cui Tao, and Degui Zhi, “Med-bert: pretrained contextualized embeddings on large-scale structured electronic health records for disease prediction,” *NPJ digital medicine*, vol. 4, no. 1, pp. 86, 2021.
- [10] Juexiao Zhou, Xiaonan He, Liyuan Sun, Jiannan Xu, Xiuying Chen, Yuetan Chu, Longxi Zhou, Xingyu Liao, Bin Zhang, Shawn Afvari, et al., “Pre-trained multi-modal large language model enhances dermatological diagnosis using skingpt-4,” *Nature Communications*, vol. 15, no. 1, pp. 5649, 2024.
- [11] Ze Liu, Yutong Lin, Yue Cao, Han Hu, Yixuan Wei, Zheng Zhang, Stephen Lin, and Baining Guo, “Swin transformer: Hierarchical vision transformer using shifted windows,” in *Proceedings of the IEEE/CVF international conference on computer vision*, 2021, pp. 10012–10022.
- [12] Yahui Xu, Yi Bin, Jiwei Wei, Yang Yang, Guoqing Wang, and Heng Tao Shen, “Multi-modal transformer with global-local alignment for composed query image retrieval,” *IEEE Transactions on Multimedia*, vol. 25, pp. 8346–8357, 2023.
- [13] Qu Yang, Mang Ye, Zhaohui Cai, Kehua Su, and Bo Du, “Composed image retrieval via cross relation network with hierarchical aggregation transformer,” *IEEE Transactions on Image Processing*, vol. 32, pp. 4543–4554, 2023.
- [14] Xuemeng Song, Haoqiang Lin, Haokun Wen, Bohan Hou, Mingzhu Xu, and Liqiang Nie, “A comprehensive survey on composed image retrieval,” *ACM Transactions on Information Systems*, vol. 44, no. 1, pp. 1–54, 2025.
- [15] Yuheng Wang, Tianze Yu, Jiayue Cai, Sunil Kalia, Harvey Lui, Z Jane Wang, and Tim K Lee, “Integrating clinical knowledge graphs and gradient-based neural systems for enhanced melanoma diagnosis via the seven-point checklist,” *IEEE Transactions on Neural Networks and Learning Systems*, 2025.
- [16] Jeremy Kawahara, Sara Daneshvar, Giuseppe Argenziano, and Ghassan Hamarneh, “Seven-point checklist and skin lesion classification using multitask multimodal neural nets,” *IEEE journal of biomedical and health informatics*, vol. 23, no. 2, pp. 538–546, 2018.
- [17] Saeed Iqbal, Adnan N Qureshi, Musaed Alhussein, Imran Arshad Choudhry, Khursheed Aurangzeb, and Tariq M Khan, “Fusion of textural and visual information for medical image modality retrieval using deep learning-based feature engineering,” *IEEE Access*, vol. 11, pp. 93238–93253, 2023.
- [18] Xin Jiang, Hao Tang, and Zechao Li, “Global meets local: Dual activation hashing network for large-scale fine-grained image retrieval,” *IEEE Transactions on Knowledge and Data Engineering*, vol. 36, no. 11, pp. 6266–6279, 2024.